Modeling DNA in Confinement: A Comparison between the Brownian Dynamics and Lattice Boltzmann Method

Y.-L. Chen,*,† H. Ma,‡ M. D. Graham,‡ and J. J. de Pablo‡

Institute of Physics and Research Center for Applied Sciences, Academia Sinica, Taipei, Taiwan, R.O.C., and Department of Chemical and Biological Engineering, University of Wisconsin—Madison, Madison, Wisconsin 53706

Received March 26, 2007; Revised Manuscript Received May 11, 2007

ABSTRACT: There is considerable interest in understanding the dynamics of complex fluids, including macromolecular solutions, in microfluidic devices. That interest has fueled the development of simulation techniques capable of describing the effect of hydrodynamic interactions in confined complex fluids. In this work, we examine the dynamics of DNA and the concomitant chain migration that arises in a parallel plate slit, at equilibrium and under pressure-driven flow. Results are presented from both the lattice Boltzmann method (LBM) and the Brownian dynamics simulations with fluctuating hydrodynamic interactions (BD-HI). It is found that the results of both methods are consistent with each other. We find that the lattice Boltzmann method is well-suited for long polymer chains as well as semidilute and concentrated DNA solutions, while Brownian dynamics is more efficient in dilute DNA solutions.

I. Introduction

Easily fabricated microfluidic devices continue to dramatically improve biochemical synthesis and analysis. In addition to the development of new fabrication techniques that have produced inexpensive sub-100 nm microfluidic channels, new devices and geometries have been explored for genome mapping, fragment separation, and manipulation of micron-sized particles, including cells.[1−10] Applications such as gene identification, oligonucleotide synthesis, and polymerase chain reaction are being performed on the microfluidic platform, with the goal of increasing throughput and lowering cost. To optimize the efficiency and functionality of the microfluidic devices, it is necessary to develop an understanding of the physics of microfluidic flow and the dynamics of biological macromolecules in such flow. In microfluidic devices having characteristic dimensions smaller than 100 μm, physics of low-Reynolds number flows are particularly relevant.

Recent single molecule experiments on DNA molecules in quiescent fluid and in flow have given new understanding of the mechanical properties of a single DNA molecule.[11−13] These measurements have facilitated the development of coarse-grained models of DNA, which have in turn provided insights into the rich dynamics of DNA molecules as they undergo pressure-driven flow in microfluidic channels.[14−17] Brownian dynamics simulations aimed at describing the extensional viscosity of dilute DNA solution and the conformation of individual molecules as they are sheared by pressure-driven flow in bulk solution have shown to be in excellent agreement with the experimental data.[18−20] These simulations have provided new insights into how DNA molecules may be manipulated in microfluidic flow. Past modeling work on DNA has also highlighted the importance of hydrodynamic interactions in microfluidic flows. More specifically, recent work has shown that accounting for hydrodynamic interaction perturbations due to the confining walls or surfaces is essential for capturing the experimentally observed migration of DNA molecules away from the walls.[21] Note, however, that available methods for Brownian simulations with fluctuating hydrodynamic inter actions exhibit a relatively unfavorable scaling with the number of interaction sites in the system. Large computational demands have therefore prevented studies of ultralong molecules or semidilute systems. This work examines the use of lattice Boltzmann methods for studies of the dynamics of semidilute DNA solutions undergoing microfluidic flow. In order to establish the validity of the lattice Boltzmann approach for studying DNA dynamics in microfluidic flow, we also present an unprecedented comparison to results of more established Brownian dynamics simulations and to experimental data.

Under pressure-driven microfluidic flow, DNA chains become extended due to the velocity gradient. Recent simulations and experiments[21−23] have found that as the DNA molecules become stretched, they migrate away from the channel walls due to the hydrodynamic interactions that arise between monomers in the vicinity of a flat surface. Recent studies by Dünweg et al.,[24,25] Ladd et al.,[26,27] and Succi et al.[28] have shown that LBM may also be applied to bulk and confined polymer solutions. Such studies, however, did not compare the results of LBM calculations to those of alternative techniques. The lattice Boltzmann method involves a number of approximations, and it is therefore of interest to examine its results in the context of different, more transparent approaches.

The lattice Boltzmann method is used in this work to examine how model DNA chains interact with the lattice fluid and to investigate the effects of flow on chain dynamics in slit microchannels. In order for LBM to capture solvent hydrodynamics, the time between solvent particle collisions must be very short compared to the time for fluid hydrodynamics to propagate in the system, so the mean free path of the solvent is much smaller than the system size, i.e., the Knudsen number $Kn \ll 1$. Recent works[29] have shown that it is possible to extend LBM to finite Kn by mimicking "virtual" collisions, allowing LBM to study the quasi-free flow regime where the solvent mean free path is comparable to the system size (nano and

* Corresponding author.
† Academia Sinica.
‡ University of Wisconsin—Madison.

10.1021/ma070729t CCC: $37.00
Published on Web 07/04/2007

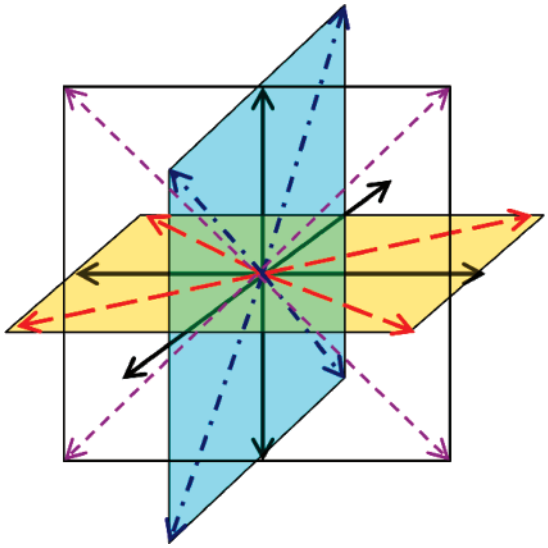

Figure 1. The 19 discrete velocities of the three-dimensional lattice Boltzmann model.

subnano systems). Microfluidic systems are well-suited for LBM modeling as the dominant length scale is micron, while the mean free path of water molecules is on the scale of nanometers. The validity of LBM in the relevant parameter regimes is addressed in the context of a coarse-grained bead−spring model of DNA, which appears to satisfy that criterion. In addition, the Schmidt number (*Sc*), the ratio between the kinematic viscosity $\nu = \eta/\rho$ (ρ is the fluid density and η is the fluid viscosity) and the coarse-grained bead diffusivity D_m, must be large so that the fluid propagates hydrodynamic interactions between beads much faster than the beads can diffuse. For molecules undergoing microfluidic flow, the competition between the inertial transport and viscous transport of the fluid is characterized by the Reynolds number $Re = \rho UH/\eta$, where U is the flow velocity. In order to observe chain migration, chain segments must be able interact with each other through hydrodynamic interactions mediated by the channel walls,[21−23,30] i.e., $Re < 1$. As shown later, the parameters chosen in our system satisfy these criteria. In this study, we will employ the LBM to study DNA systems by coupling fluctuating molecular dynamics with LBM through the bead−fluid friction force. We will compare the LBM results for chain relaxation and chain migration to the Brownian dynamics and experimental results.

II. Lattice Boltzmann Methodology

The lattice Boltzmann method has been well described in numerous recent review articles.[31−34] Only a concise description is provided here. Instead of solving for the fluid dynamics in continuum, the LBM solves the fluid mass and momentum conservation equations on a lattice in both position and velocity space. We employ a three-dimensional lattice, where each lattice site has 19 discrete velocities (D3Q19).[34] The 19 discrete velocities $\mathbf{c}_i$ are given by (0,0,0), (±1,0,0), (0,±1,0), (0,0,±1), (±1,±1,0), (±1,0,±1), and (0,±1,±1), as illustrated in Figure 1. The magnitudes of the velocities are $c_i = |\mathbf{c}_i| = 0$, 1, and $\sqrt{2}$. The lattice simulation has grid size Δx and timestep $\Delta\tau$. The maximum velocity in the simulation is the speed of sound $c_s = \sqrt{1/3}\Delta x/\Delta\tau$. The velocity distribution function $n_i(\mathbf{r},t)$ gives the fluid population with the velocity $\mathbf{c}_i$ at position $\mathbf{r}$ at time t. At equilibrium, the velocity distribution functions can be represented as a second-order expansion of the Maxwell−Boltzmann distribution, given by[32,34]

$$n_i^{eq}(r,t) = \rho a^{c_i}[1 + (\mathbf{c}_i\cdot\mathbf{u})/c_s^2 + \mathbf{uu}:(\mathbf{c}_i\mathbf{c}_i - c_s^2\mathbf{I})/(2c_s^4)] \quad (1)$$

$$\rho = \sum_i n_i^{eq}, \quad \rho\mathbf{u} = \sum_i \mathbf{c}_i n_i^{eq}, \quad \Pi = \rho(\mathbf{uu} + c_s^2\mathbf{I}) = \sum_i n_i^{eq}\mathbf{c}_i\mathbf{c}_i \quad (1a)$$

$$\sum_i a^{c_i} c_{i\alpha}c_{i\beta}c_{i\gamma}c_{i\delta} = c_s^4(\delta_{\alpha\beta}\delta_{\gamma\delta} + \delta_{\alpha\gamma}\delta_{\beta\delta} + \delta_{\alpha\delta}\delta_{\beta\gamma}) \quad (1b)$$

The indices α, β, γ, δ denote axis x, y, and z. $\mathbf{u}$ is the local velocity, and the coefficients a^{c_i} are determined by satisfying the equilibrium conditions in eq 1a and the isotropy condition in eq 1b.[32] For our D3Q19 system, $a^0 = 1/3$, $a^1 = 1/18$, and $a^{\sqrt{2}} = 1/36$. In terms of the fluid hydrodynamic properties, the velocity distribution functions are transformed to the hydrodynamic moments, $M_q = \mathbf{m}\cdot\mathbf{n}$, where M_q is the qth moment of $\mathbf{n} = (n_0, n_1, ..., n_{18})$ and $\mathbf{m}$ is the transformation matrix. The 19 moments of the velocity distribution function are the density ρ, the momentum density $\mathbf{j} = \rho\mathbf{u}$, the momentum flux $\Pi = \rho(\mathbf{uu} + c_s^2\mathbf{I})$, and the kinetic energy fluxes, which conserve energy ("ghost" moments).

At each time step, the fluid particles undergo local collision at the lattice site, and the velocity distribution functions evolve as

$$n_i(\mathbf{r} + \mathbf{c}_i\,dt, t + dt) = n_i(\mathbf{r},t) + L_{ij}[n_j(\mathbf{r},t) - n_j^{eq}(\mathbf{r},t)] \quad (2)$$

where L is a collision operator for dissipation due to fluid particle collisions such that the fluid always relaxes toward the equilibrium distribution. Local dissipation of the fluid momentum is justified if the particle mean free path is much shorter than the lattice size, i.e., $Kn \ll 1$. For small Kn and Mach number ($Ma = u/c_s$), eq 2 has been shown to be equivalent to the Navier−Stokes equation.[33]

The simplest choice of the collision operator is a diagonal matrix with diagonal elements (τ_0^{-1}, τ_1^{-1}, τ_2^{-1},..., τ_{18}^{-1}), where τ_q is the characteristic relaxation time of the hydrodynamic moment q. For the conserved moments (ρ and $\rho\mathbf{u}$), the relaxation time is infinite and $\tau_q^{-1} = 0$. There are several studies that investigate the differences between a multiple relaxation time simulation and simpler models,[33,35,36] and the debate is ongoing. For simplicity, we choose the Bhatnagar−Gross−Krook (BGK) model[37] with a single relaxation time $\tau_q^{-1} = \tau_s^{-1}$ for the momentum flux moments. The fluid shear viscosity can be shown to be related to the relaxation time[33,34] by $\eta = \rho c_s^2(\tau_s - 0.5)$, where $\tau_s > 0.5$. A constraint on the fluid relaxation time is that it must be shorter than the fluid momentum diffusion time across the system, i.e., $\tau_s < \rho H^2/\eta$, which leads to $\tau_s < 2$ for $H = \Delta x$. However, the box size is typically larger than $5\Delta x$.

For the DNA chain, we use a model employed in previous Brownian dynamics simulations[16−18] that is based on the elasticity and diffusivity of 48.5 kbps YOYO-stained λ-DNA. The molecule is represented by a collection of beads and springs. In the LBM simulations, the beads are viewed as point forces that interact with the fluid. The model λ-DNA chain has $N_s = 10$ springs with $N_{ks} = 19.8$ Kuhn segments per spring, and the Kuhn segment length $\sigma_k = 0.106$ μm. The contour length of the chain is $L = N_{ks}N_s\sigma_k = 21.2$ μm. The beads interact solely through the excluded volume interactions between the beads, the elasticity of the chain, the hydrodynamic interactions between beads through the solvent, and the Brownian motion of the chain due to chain−solvent interactions.

The position and velocity of the coarse-grained beads are updated using the explicit Euler method, given by

$$\mathbf{u}(t+\Delta t) = \mathbf{u}(t) + \mathbf{f}(t)\Delta t/m$$
$$\mathbf{x}(t+\Delta t) = \mathbf{x}(t) + \mathbf{u}(t)\Delta t \quad (3)$$

where $\mathbf{f}(t)$ represents the forces acting on the beads of mass m and Δt is the time step. The excluded volume interaction between the chain segments can be calculated by assuming that short chain segments behave as ideal random walks; the interbead interaction can therefore be expressed as a Gaussian excluded volume potential with the form

$$U_{ij}^{ev} = \frac{1}{2} k_B T \upsilon N_{ks}^{\ 2} \left(\frac{3}{4\pi S_s^{\ 2}}\right)^{3/2} \exp\left(\frac{-3|\mathbf{r}_i - \mathbf{r}_j|^2}{4S_s^{\ 2}}\right) \quad (4)$$

where $\upsilon = \sigma_k^3$ is the excluded volume interaction parameter, N_{ks} is the number of Kuhn segments per spring, and $S_s^2 = (N_{ks}/6)\sigma_k^2$ is the characteristic size of the coarse-grained beads. The excluded volume interaction leads to self-avoiding walk chain statistics. Chain elasticity is obtained through the wormlike chain springs that connect adjacent beads. The force−extension dependence of the DNA chain has been measured by experiments[38,39] and shown to fit

$$\mathbf{f}_{ij}^{s} = \frac{k_B T}{2\sigma_k}\left[\left(1 - \frac{|\mathbf{r}_j - \mathbf{r}_i|}{N_{ks}\sigma_k}\right)^{-2} - 1 + 4\frac{|\mathbf{r}_j - \mathbf{r}_i|}{N_{ks}\sigma_k}\right]\frac{\mathbf{r}_j - \mathbf{r}_i}{|\mathbf{r}_j - \mathbf{r}_i|} \quad (5)$$

Although this force−extension relation applies for the entire chain, in our model we will assume it also applies for chain segments that are of sufficient number of Kuhn lengths. The beads are coupled to the fluid through the friction force exerted on the beads,[24] given by

$$\mathbf{F}_f = -\zeta(\mathbf{u}_p - \mathbf{u}_f) \quad (6)$$

$\zeta = 6\pi\eta a$ is the friction coefficient, and $\mathbf{u}_p - \mathbf{u}_f$ is the particle velocity relative to the fluid velocity. The fluid velocity at the particle position is determined by trilinear interpolation of the fluid velocity $\mathbf{u}_i^{(nn)}$ of the neighboring lattice sites (nn):

$$\mathbf{u}_f(\mathbf{r}) = \sum_{i\in(nn)} w_i \mathbf{u}_i^{(nn)} \quad (7)$$

The weighting functions w_i are the normalized Lagrange interpolation polynomials through the bead's neighbor lattice site i. For example, for a particle in between sites x_0 and x_1 on a line

$$u_f(x) = \frac{x - x_0}{x_1 - x_0} u_f(x_1) + \frac{x - x_1}{x_1 - x_0} u_f(x_0) \quad (8)$$

$\mathbf{u}_i$ is the fluid velocity at the neighbor lattice site i. The momentum exchanged between the fluid and the bead, $\Delta j = -\mathbf{F}_f\Delta t/\Delta x^3$, is distributed to the neighboring lattice sites with the same weighting functions w_i used in the trilinear interpolation. For velocity q on the neighbor site i, the momentum transfer is given by

$$\Delta\mathbf{f}_i = w_i a^{c_i} \Delta\mathbf{j}\cdot\mathbf{c}_q/c_s^{\ 2} \quad (9)$$

The monomer−fluid coupling has been verified by comparing the present calculations with Figures 2 and 4 of ref 27.

Fluid thermal fluctuations in lattice Boltzmann simulations can be accounted for through adding random stresses to the fluid via the method of Ladd et al.[31] or that of Adhikari et al.[40] The fluid thermal fluctuations affect particle Brownian motion only when explicit fluid−solid boundary conditions are implemented. In this work, we use point force beads, and it has been shown in previous studies[24] that the bead−fluid coupling given in eq 6 dissipates the fluid thermal fluctuations, and the bead−fluid fluctuation is only correctly accounted for when the detailed fluid−solid boundary conditions are applied.[31] Instead, a bead Brownian force that satisfies the fluctuation−dissipation theorem is included in our equation of motion. The bead force fluctuations have a Gaussian distribution with zero mean, and the variance is $2kT\zeta/\Delta t$.

To simulate pressure-driven flow in the microchannel, a pressure gradient is introduced in the LBM by adding an external momentum density to the distribution function n_i. A bias is added to the velocity distribution function n^{ext} to all the lattice sites,[31] given by

$$n_i(\mathbf{r} + \mathbf{c}_i\,\mathrm{d}t,\, t + \mathrm{d}t) = n_i(\mathbf{r},t) + L_{ij}[n_i(\mathbf{r},t) - n_i^{eq}(\mathbf{r},t)] + n^{ext}(\mathbf{r},t) \quad (10)$$

By calculating an effective shear rate $\dot\gamma = u_{max}/(H/2)$, the Weissenberg number $We = \dot\gamma\tau_{relax}$ can then be determined from the maximum velocity of the parabolic velocity profile, where τ_{relax} is the DNA relaxation time and H is the channel height. Our prior studies found that the DNA molecules stretch only when $We > 1$.[17] We are thus constrained to choose systems where $We > 1$ and the Reynolds number $Re = u_{max}H/\nu < 1$. For a 10 μm high channel, water-filled microfluidic channel, the maximum fluid velocity at $Re = 1$ is $u_{max} = 0.1$ m/s. From the experimentally determined relaxation time of λ-DNA in 1 cP solvent (water) of 0.095 s, we find that the upper limiting value of the Weissenberg number is ~2000. Prior experiments and simulations have found that the average chain stretch reaches a plateau for $We \sim 40$, and we will not investigate flow conditions above $We = 100$.

III. Results

A. Simulation Length and Time Scale. For all lattice Boltzmann simulations, there persists the question of how the time and the length scale of the lattice fluid relate to the physical phenomena being studied.[41,42] In our system, the relevant physical length and time scales are the radius of gyration (R_g) and the relaxation time (τ_{relax}) of the DNA molecule. For the much studied λ-DNA molecule, $R_g = 0.7$ μm and $\tau_{relax} = 0.095$ s in water, and the lattice spacing and simulation time steps must scale accordingly. Given the fluid kinematic viscosity $\nu = 1/6$ in the lattice units of $\Delta x^2/\Delta\tau$, a reasonable time step $\Delta\tau = 10^{-3}\tau_{relax}$ may be chosen such that the momentum transfer between polymer and fluid is accurately modeled. For water at room temperature, $\nu = 10^{-6}$ m^2/s. Matching the water kinematic viscosity with the simulation value leads to a grid size $\Delta x \approx 25$ μm, which is too large compared to R_g. The simulation grid size should be of approximately same length as the average spring length to capture the hydrodynamic interactions between intrachain segments. The experimentally measured radius of gyration of λ-DNA of 0.7 μm would correspond to an average spring length of 0.52 μm for our model DNA with 10 springs. We are thus justified in choosing a lattice spacing of $\Delta x = 0.5$ μm.[18,25] With this lattice spacing and $\nu = 1/6$, the hydrodynamic radius of the coarse-grained bead is $0.154\Delta x$, which leads to the friction coefficient $\zeta = 6\pi\eta a = 0.483\rho[m_0/\Delta\tau]$, where m_0 is the mass unit of a fluid particle determined from the simulation fluid density $\rho = 36m_0/\Delta x^3$ matched to the density of water.

We now discuss the choice of the simulation parameters. Given $\Delta x = 0.5$ μm and $\Delta t = 10^{-3}\tau_{relax}$, the water kinematic

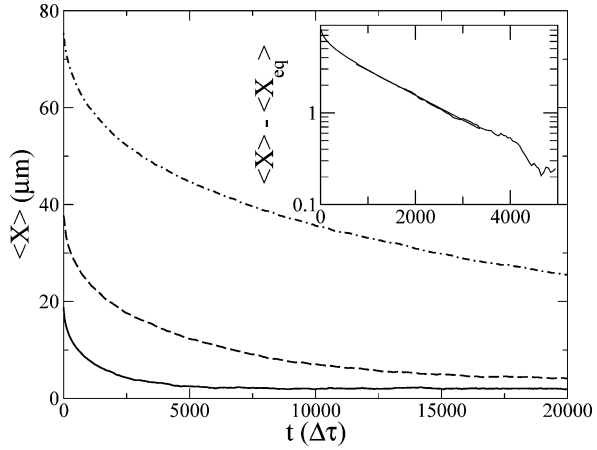

Figure 2. Relaxation of a fully stretched model DNA chain in bulk solution for $N_s = 10$ (solid line), 20 (dashed line), and 40 (point dashed line). The simulation parameters are $\nu = 1/6$, $\zeta = 0.483\rho$, and $kT/\zeta = 10^{-3}$ in a box of $1.5L \times 30 \times 30$ $(\Delta x)^3$. The inset shows the exponential fit (dark solid line) for the $N_s = 10$ chain relaxation.

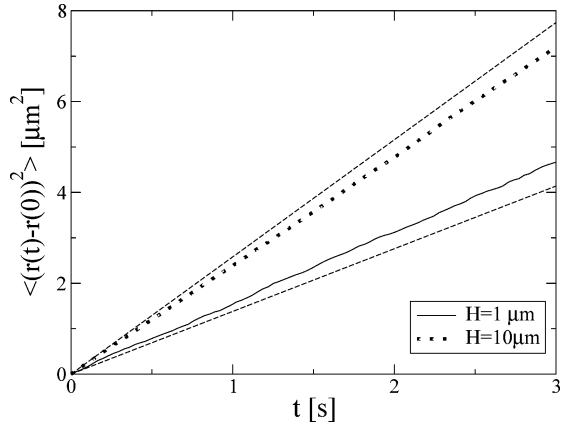

Figure 3. Diffusion of model DNA chains in slit confinement for $N_s = 10$ and $H = 1$ (μm (solid line) and 10 μm (dotted line). The simulation parameters are $\nu = 1/6$, $\zeta = 0.483\rho$, and $kT/\zeta = 10^{-3}$. Dashed lines are the chain mean-square displacement calculated from the experimental diffusion coefficients.

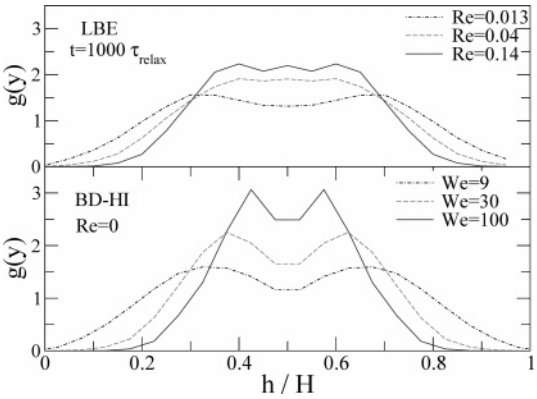

Figure 4. Bead distribution profile in the channel cross section from LBM for $N_s = 10$ and $We = 100$ in the 10 μm slit channel after $1000\tau_{relax}$ and $100\tau_{relax}$. The error bars are less than 10% of the value. The LBM parameters are $\nu = 1/6$, $\zeta = 0.483\rho$, and $kT/\zeta = 10^{-3}$, 10^{-4}, and 10^{-5}, corresponding to Re = 1.4, 0.14, and 0.014.

viscosity is $3800[\Delta x^2/\Delta\tau]$, which is outside the hydrodynamic limit of the LBM simulation as the fluid cannot relax to equilibrium. If we match the simulation kinematic viscosity and density to that of water at room temperature, the simulation step is found to be $\Delta\tau = 4.17 \times 10^{-8}$ s. This gives a simulation energy scale of $e_0 = m_0\Delta x^2/\Delta\tau^2 = 5 \times 10^{-16}$ J, $kT = 8.3 \times 10^{-6}e_0$, and $D_m = kT/\zeta = 4.7 \times 10^{-7}\ \Delta x^2/\Delta\tau$. For a λ-DNA in a 10 μm high channel and pressure-driven flow with $We = 100$, $u_{max} = 5 \times 10^3$ μm/s $= 4.17 \times 10^{-4}\Delta x/\Delta\tau$. The dimensionless groups are $Re = 0.05$, $Ma = 7.6 \times 10^{-4}$, and $Sc = \nu/D = \nu\zeta/kT = 3.5 \times 10^5$, which are well within the valid regime of the LBM simulation. However, a simulation of one chain relaxation time would take 2.4×10^6 steps and ~24 h on a 3.4 GHz Pentium 4 CPU with a moderate system size of $40 \times 20 \times 40$ (Δx^3). The phenomenon of hydrodynamic migration in microchannels reaches steady state at $t \sim H^2/D_{chain}$, which is typically greater than 100 chain relaxation times for $H = 10$ μm. Thus, a simulation to achieve the steady-state chain migration profile has a very high computational cost. Instead, we can choose parameters that still satisfy the criteria $Sc \gg 1$, $Ma \ll 1$, and $Re < 1$ and at the same time allowing the chain molecule to relax faster within the simulation.

If we increase the diffusivity of the chain, the chain dynamics can be captured in a reasonable simulation time. The LBM parameters are $\nu = 1/6$, $\zeta = 0.483\rho$, and $D_m = kT/\zeta = 10^{-3}$, which leads to $\Delta\tau = 8.8 \times 10^{-5}$ s and $Sc = 167$. For the Brownian motion of the coarse-grained beads, we choose the integration time step to be $\Delta\tau = 0.01$ in eq 3, and the lattice Boltzmann updates of the fluid velocity distributions are performed every five Brownian dynamics steps. The chain stretch, radius of gyration, diffusivity, and relaxation times are calculated for $N_s = 5$, 10, 20, and 40 in periodic boxes of $30 \times 30 \times 30$. The radius of gyration of the chains are found to be $R_g = 0.5$, 0.76, 1.16, and 1.75 μm. The scaling exponent of 0.6 is in agreement with scaling theory predictions for polymers in good solvent, and the results agree quantitatively with the Brownian dynamics simulations. Figure 2 shows the average chain stretch (X = maximum dimension of the chain) of initially fully stretched DNA chains as the chains are allowed to relax in a rectangular simulation box of size $2\ L \times 30 \times 30$. The chain relaxation time for $N_s = 10$ can be extracted by fitting the exponential decay region to $\exp(-t/\tau_{relax})$, and τ_{relax} is found to be $1600\Delta\tau$.

We also performed simulations of DNA chains in static slit confinement to determine the diffusivity of the DNA molecules. The chain center-of-mass mean-squared displacement, i.e., $\langle(r(t) - r(0))^2\rangle$, shown in Figure 3 allows us to calculate the chain diffusivity $D = \langle(r(t) - r(0))^2\rangle/(6t)$ in the parallel slit for $R_g < H$. For the $N_s = 10$ chain (λ-DNA), we found chain diffusivities of $D = 0.38$ and 0.24 μm^2/s in $H = 10$ and 1 μm parallel slit channels, respectively. These values are in agreement with experimental values of 0.43 and 0.21 μm^2/s, validating the LBM parameters we have chosen. We can now proceed to study the DNA dynamics under pressure-driven flow in parallel plate slit microchannels and compare the results with BD-HI simulations.

B. Pressure-Driven Microfluidic Flow. Brownian dynamics simulations accounting for wall hydrodynamic effects have also been performed to compare the results with LBM. In Brownian dynamics, the hydrodynamic interactions are first solved by the finite element method[16,23] or other methods[43,44] and then coupled to the chain dynamics. Details of the BD-HI simulations have been given in prior publications and will not be described here.[18] We first performed the calculation with a single model λ-DNA chain in a parallel slit channel $H = 10$ μm undergoing pressure-driven flow of $We = 9$, 30, and 100. Figure 4 shows the chain distribution as a function of the chain center-of-mass position after the DNA molecules have undergone pressure-driven flow for $1000\tau_{relax}$, after the chain distribution in the channel has reached steady state. We observe strong DNA migration toward the channel center as We increases. The off-center chain

Table 1. Dimensionless Groups in the LBM Simulations and in a 10 μm Microchannel with Water as the Solvent

D_m ($\Delta x^2/\Delta\tau$)	We	*Re* (sim)	*Re* (real)	*Sc* (sim)	*Sc* (real)
10^{-3}	100	1.4	0.05	1.7×10^2	3.5×10^5
10^{-4}	100	0.14	0.05	1.7×10^3	3.5×10^5
10^{-4}	30	0.04	0.015	1.7×10^3	3.5×10^5
10^{-4}	9	0.013	0.0045	1.7×10^3	3.5×10^5
10^{-5}	100	0.014	0.05	1.7×10^4	3.5×10^5

distribution peak is due to the competition between the migration toward the center and the lower chain mobility away from channel center. This is also consistent with prior simulations in square channels.[21−23]

We also performed lattice Boltzmann simulation for DNA molecules undergoing flow under the same conditions as the BD-HI simulation for 50 DNA chains (550 beads). The LBM simulations box corresponding to the 10 μm high channel has the dimensions of $L_x = L_z = 40\Delta x$ and $L_y = H = 20\Delta x$. This polymer concentration corresponds to $c_p/c_p^* = 0.02$, where $c_p^* = 1/(4/3\pi R_g^3)$ is the dilute−semidilute crossover of the chain molecules. The boundary conditions are periodic in the *x* and *z* directions, and the walls are in the *y* direction by the addition of a short-ranged cubic potential for the beads and the bounce-back condition for the lattice fluid.

For DNA molecules undergoing pressure-driven flow, choosing the LBM parameters requires much more care. We want to simulate conditions where the geometry and the flow are defined with fixed *H* and *We*. In order to satisfy the criteria $Re \sim WeH^2kT/(a\eta^2) < 1$, $Ma \sim WeHkT/(\eta a) \ll 1$, and $Sc \sim \eta^2 a/kT \gg 1$, we chose to change *kT* to reduce the simulation time and examine how they affect chain dynamics. The dimensionless groups change with *kT*, and they are tabulated in Table 1.

Starting with the idea that a simulation time step $\Delta\tau = 10^{-3}\tau_{relax} \sim 10^{-4}$ s should accurately model the momentum transfer between the chain molecule and the fluid, this choice of $\Delta\tau$ reduces the simulation time by 3 orders of magnitude when we compare it to the case if the kinematic viscosity is matched to that of water with $\Delta\tau = 4 \times 10^{-8}$ s. Brownian forces are added to the beads with the Stokes−Einstein diffusivity $D_m = kT/\zeta = 10^{-3}$. These parameters give $\Delta\tau = 8.8 \times 10^{-5}$ s. However, under pressure-driven flow with $We = 100$, the Reynolds number of the simulation is ∼1.4. At such moderate *Re*, hydrodynamic interactions between the DNA due to the channel walls may not have time to influence the dynamics of the DNA molecules.[45] To reduce the Reynolds number at a fixed *We*, we further decrease D_m and examine the cases for $D_m = 10^{-3}$ ($Re = 1.4$), $D_m = 10^{-4}$ ($Re = 0.14$), and 10^{-5} ($Re = 0.014$). As shown in Figure 5, the steady state bead distribution profile in the channel cross section does not change as D_m and the *Re* decrease at $We = 100$. However, Figure 5 shows that at $t = 100\tau_{relax}$ the transient chain migration effect increases slightly as D_m decreases. In particularly, the off-center peaks in the bead density profile increase in magnitude as D_m decreases due to the chain migration toward the walls from the channel center. This suggests that even at a moderate Reynolds number ∼ 1, LBE predicts the chain migration away from the confining walls. The balance between choosing a minimum simulation time and studying the relevant physical regime may be achieved with a larger time step than if the LBE fluid is strictly matched to the water viscosity. The dimensionless groups in the calculations are tabulated in Table 1.

To compare the LBE to the BD-HI simulations, the LBE parameters $\nu = 1/6$, $\zeta = 0.483\rho$, and $D_m = 10^{-4}$ are chosen. Figure 4 shows the steady state bead density profile in the slit channel cross section of the DNA chains after undergoing pressure-driven flow for 1000 chain relaxation times. As *We* increases, a stronger chain migration effect is observed in both LBE and BD-HI. It is found that the DNA depletion layer thickness, defined as the distance between the half-maximum-height position and the wall, predicted by LBM is smaller than that predicted using BD-HI. The same trend is also observed under transient conditions where the chain density distribution in the channel cross section has not reached steady state. This may be attributed to the condition of finite Reynolds number which exists in the LBE and not in BD-HI. The trend of stronger depletion as Reynolds number decreases is also suggested by the transient results shown in Figure 5.

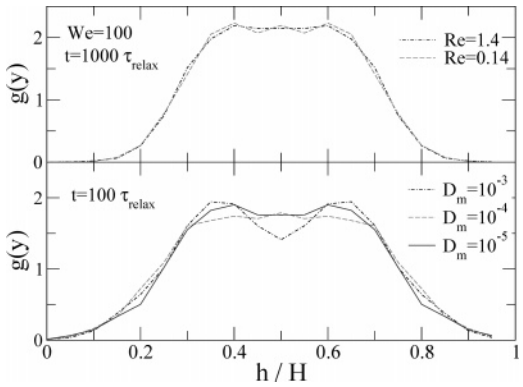

Figure 5. Bead distribution profile in the channel cross section from LBM and BD-HI for $N_s = 10$ and $We = 9$, 30, and 100 in the 10 μm slit channel after $1000\tau_{relax}$.

C. Nondilute Conditions. Prior comparison between LBM and traditional molecular dynamics of pure fluids has estimated that the LBM method provides a speedup of more than an order of magnitude.[25] For polymer solutions, the lattice Boltzmann simulation is not always more efficient than the Brownian dynamics. The major reason is that the lattice Boltzmann simulation cost depends linearly on the size of the three-dimensional lattice. The lattice spacing must be small enough such that the simulations can capture the polymer dynamics, and at the same time the simulation parameters must be in the physically relevant domain. To capture phenomena such as chain migration due to hydrodynamic interactions between beads, the grid size of the lattice Δx depends on the number of Kuhn segments per spring and the average length of the spring, and this restricts the size of the simulation box.

We have used a Pentium 4, 3.4 GHz computer with 2 GB of memory for comparing the computational time between LBM and BD-HI. For the $40 \times 20 \times 40$ Δx^3 simulation box, the computational time to complete one chain relaxation with a LBM time step $\Delta\tau = 8.8 \times 10^{-6}$ ($D_m = 10^{-4}$) is ∼400 s. A BD time step of $\Delta t = 0.01$ is used in the explicit integration scheme for the LBM simulations, while a $\Delta t = 0.025$ is used in the BD-HI simulations in a semi-implicit scheme. Figure 6 compares the computation time (t_{cpu}) for one chain relaxation time of λ-DNA molecules. We find, as expected, that t_{cpu} for LBM depends very weakly on the number of particles, and t_{cpu} for BD-HI $\sim t^{1.9}$. As a result, we find that for this system size the LBM method becomes more efficient than BD-HI when the number of beads $N > 150$. For the model λ-DNA, this corresponds to a polymer concentration of $c_p/c_p^* = 0.006$. In order to study concentration effects up to the dilute−semidilute crossover, we employ the LBM method.

Figure 7 shows the concentration profile of DNA chains undergoing microfluidic flow at chain concentrations below the dilute−semidilute crossover. LBE is used to investigate DNA

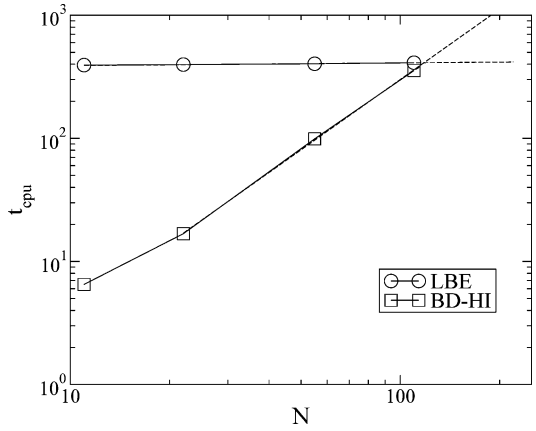

Figure 6. Computational times of LBM in a simulation box of 30 × 30 × 30 and BD-HI for one λ-DNA relaxation time. Dashed lines are extrapolations from fitting.

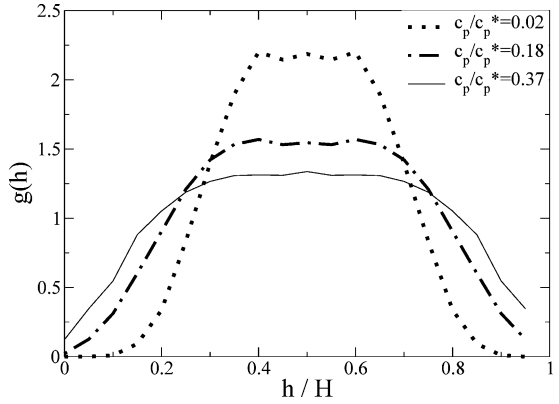

Figure 7. Bead distribution profile in the channel cross section from LBM for $N_s = 10$ and $We = 100$ in the 10 μm slit channel at steady state for $N = 550$, 4400, and 8800, corresponding to $c_p/c_p^* = 0.023$, 0.18, and 0.37. The LBM parameters are $\nu = 1/6$, $\zeta = 0.483\rho$, and $kT/\zeta = 10^{-4}$. The error bars are less than 10% of the value.

chains at concentrations of $c_p/c_p^* = 0.02$, 0.18, and 0.37 in Poiseuille flow inside a 10 μm slit channel with $\nu = 1/6$, $D_m = 10^{-4}$, and $We = 100$. It is found that the depletion layer decreases as the DNA concentration increases, which may be attributed to excluded volume interactions between DNA chains that have migrated toward the channel center, as well as screening of the inter-DNA hydrodynamic interactions due to the higher local concentration in the channel center. As c_p/c_p^* increases from 0.02 to 0.37, the depletion layer thickness decreases from 2.3 to 1.1 μm. Such an effect is observable using optical microscopy with fluorescently labeled DNA molecules. Another consequence of increasing chain concentration is the reduced average velocity of the DNA molecules. Chain migration toward the channel center suggests that in Poiseuille flow the average DNA velocity would be higher than the average fluid velocity. As the DNA concentration increases, the chain migration effect is reduced by inter-DNA repulsion, leading to the decrease of average DNA velocity.

IV. Discussion

In this work, we have shown that the LBM method can be highly useful for understanding the dynamics of DNA molecules in microfluidic flow, given that care is taken for choosing the simulation parameters. As with other simulation methods that attempt to span a large separation of length and time scales, the parameters chosen in our simulations necessarily focus on long-range, large time scale effects such as the flow-induced chain migration phenomenon and neglect nanosecond scale aspects of the DNA−fluid interaction. A key difference between the Brownian dynamics calculations and the LBM calculations is that the inertial effects are neglected in Brownian dynamics. In BD-HI, the microfluidic flow is always considered to have $Re = 0$, and hydrodynamic interactions between beads are assumed to propagate instantly. Neglecting inertial effects in microfluidic flow is generally justified because $Re \ll 1$, such as in our model system of λ-DNA undergoing pressure-driven flow in a 10 μm slit microchannel where $Re = 0.05$ when $We = 100$. In our LBM simulations, we have carefully chosen our simulation parameters such that the $Sc \gg 1$ so that hydrodynamic interactions propagate faster than the bead diffusion, and Re is small such that wall perturbations of the bead hydrodynamic interactions affect the dynamics of DNA chains. Although we still observe differences in the steady-state chain migration between LBM and BD-HI, these can be attributed to the discrete lattice size and the finite momentum propagation time in the LBM simulations. The propagation of hydrodynamic interactions is instantaneous in the BD-HI, while it is of finite time in the LBM simulations. Although inertial effects do not affect the qualitative behavior, our study suggests that they may affect the chain migration density profile quantitatively.

Our comparison for computational efficiency showed that for dilute DNA suspensions the lattice Boltzmann simulation is not always the most efficient. For our choice of system parameters, the LBM becomes more efficient and faster than the BD-HI method of Jendrejack et al.[18] only when the number of particles is greater than 150. However, further reduction of LBM simulation time may be made by optimizing the system parameters such that we choose the smallest box size possible while retaining the optimum accuracy. The LBM method is very promising in this respect, and we expect that future investigations of dense polymer solutions with LBM will allow us to answer challenging problems about the polymer rheology in confinement, as well as polymer dynamics in channels of nonsimple geometry. Studying denser polymer solutions undergoing microfluidic flow using LBM will also allow us to address how interchain interactions affect the migration dynamics of DNA molecules.

Acknowledgment. We thank Professor A. Ladd and Dr. O. B. Usta for providing the fluid lattice Boltzmann program and their helpful advice regarding their lattice Boltzmann code. We also thank Prof. D. C. Schwartz, Dr. O. Guzman, and Mr. M. Chopra for insightful discussions on DNA dynamics in the microchannel. Y.L.C. is grateful to the NIH for a UW-GSTP fellowship. This work was supported by the UW-NSEC on Directed Assembly.

References and Notes

(1) Marziali, A.; Akeson, M. *Annu. Rev. Biomed. Eng.* **2001**, *3*, 195.
(2) Odom, T. W.; Thalladi, V. R.; Love, J. C.; Whitesides, G. M. *J. Am. Chem. Soc.* **2002**, *124*, 12112.
(3) Shrewsbury, P. J.; Muller, S. J.; Liepmann, D. *Biomed. Microdevices* **2001**, *3*, 225.
(4) Wei, C.-W.; Cheng, J.-Y.; Huang, C.-T.; Yen, M.-H.; Young, T.-H. *Nucleic Acids Res.* **2005**, *33*, e78.
(5) Whitesides, G. M.; Ostuni, E.; Takayam, S.; Jiang, Z.; Ingber, D. E. *Annu. Rev. Biomed. Eng.* **2001**, *3*, 335.
(6) Reisner, W. W.; Austin, R. H. *Phys. Rev. Lett.* **2005**, *94*, 196101.
(7) Tegeneldt, J. O.; Prinz, C.; Cao, H.; Chou, S.; Reisner, W. W.; Riehn, R.; Wang, Y. M.; Cox, E. C.; Sturm, J. C.; Silberzan, P.; Austin, R. H. *Proc. Natl. Acad. Sci. U.S.A.* **2004**, *101*, 10979.
(8) Tegeneldt, J. O.; Prinz, C.; Cao, H.; Huang, R. L.; Austin, R. H.; Chou, S. Y.; Cox, E. C.; Sturm, J. C. *Anal. Bioanal. Chem.* **2004**, *378*, 1678.

(9) Dendukuri, D.; Tsoi, K.; Hatton, T. A.; Doyle, P. S. *Langmuir* **2005**, *21*, 2113.
(10) Randall, G. C.; Doyle, P. S. *Phys. Rev. Lett.* **2004**, *93*, 058102.
(11) Smith, D. E.; Babcock, H. P.; Chu, S. *Science* **1999**, *283*, 1724.
(12) Smith, D. E.; Chu, S. *Science* **1998**, *281*, 1335.
(13) Bustamante, C.; Bryant, Z.; Smith, S. B. *Nature (London)* **2003**, *421*, 423.
(14) Chen, Y.-L.; Graham, M. D.; de Pablo, J. J.; Randall, G. C.; Gupta, M.; Doyle, P. S. *Phys. Rev. E* **2004**, *70*, 060901.
(15) Hsieh, C. C.; Li, L.; Larson, R. G. *J. Non-Newtonian Fluid. Mech.* **2003**, *113*, 147.
(16) Jendrejack, R. M.; Dimalanta, E. T.; Schwartz, D. C.; Graham, M. D.; de Pablo, J. J. *Phys. Rev. Lett.* **2003**, *91*, 038102.
(17) Jendrejack, R. M.; Schwartz, D. C.; Graham, M. D.; de Pablo, J. J. *J. Chem. Phys.* **2003**, *119*, 1165.
(18) Jendrejack, R. M.; de Pablo, J. J.; Graham, M. D. *J. Chem. Phys.* **2002**, *116*, 7752.
(19) Shaqfeh, E. S. G. *J. Non-Newtonian Fluid. Mech.* **2004**, *130*, 2005.
(20) Larson, R. G.; Hu, H.; Smith, D. E.; Chu, S. *J. Rheol.* **1999**, *43*, 267.
(21) Jendrejack, R. M.; Schwartz, D. C.; de Pablo, J. J.; Graham, M. D. *J. Chem. Phys.* **2004**, *120*, 2513.
(22) Chen, Y.-L.; Jo, K.; Graham, M. D.; Schwartz, D. C.; de Pablo, J. J. *Macromolecules* **2005**, *38*, 6680.
(23) Ma, H.; Graham, M. D. *Phys. Fluids* **2005**, *17*, 083103.
(24) Ahlrichs, P.; Dünweg, B. *Int. J. Mod. Phys. C* **1998**, *9*, 1429.
(25) Ahlrichs, P.; Dünweg, B. *J. Chem. Phys.* **1999**, *111*, 8225.
(26) Usta, O. B.; Ladd, A. J. C.; Butler, J. E. *J. Chem. Phys.* **2005**, *122*, 094902.
(27) Usta, O. B.; Butler, J. E.; Ladd, A. J. C. *Phys. Fluids* **2006**, *18*, 031703.
(28) Fyta, M.; Melchionna, S.; Kaxiras, E.; Succi, S. *Multiscale Model. Simul.* **2006**, *5*, 1156.
(29) Toschi, F.; Succi, S. *Europhys. Lett.* **2005**, *69*, 549.
(30) Hernández-Ortiz, J.-P.; Ma, H.; de Pablo, J. J.; Graham, M. D. *Phys. Fluids* **2006**, *18*, 123101.
(31) Ladd, A. J. C. *J. Fluid. Mech.* **1994**, *271*, 285.
(32) Ladd, A. J. C.; Verberg, R. *J. Stat. Phys.* **2001**, *104*, 1191.
(33) Benzi, R.; Succi, S.; Vergassola, M. *Phys. Rep.* **1992**, *222*, 145.
(34) Succi, S. *The Lattice Boltzmann Equation for Fluid Dynamics and Beyond*, 1st ed.; Oxford University Press: Oxford, 2001.
(35) D'Humieres, D.; Ginzburg, I.; Krafczyk, M.; Lallemand, P.; Luo, L.-S. *Philos. Trans. R. Soc. London A* **2002**, *360*, 437.
(36) Higuera, F.; Succi, S.; Benzi, R. *Europhys. Lett.* **1989**, *9*, 345.
(37) Bhatnagar, P.; Gross, E. P.; Krook, M. K. *Phys. Rev.* **1954**, *94*, 511.
(38) Smith, S. B.; Finzi, L.; Bustamante, C. *Science* **1992**, *258*, 1122.
(39) Marko, J. F.; Siggia, E. D. *Macromolecules* **1994**, *28*, 8759.
(40) Adhikari, R.; Stratford, K.; Cates, M. E.; Wagner, A. J. *Europhys. Lett.* **2005**, *71*, 473.
(41) Cates, M. E.; Desplat, J.-C.; Stansell, P.; Wagner, A. J.; Stratford, K.; Adhikari, R.; Pagonabarraga, I. *Philos. Trans. R. Soc. London A* **2005**, *363*, 1917.
(42) Horbach, J.; Succi, S. *Phys. Rev. Lett.* **2006**, *96*, 224503.
(43) Hernández-Ortiz, J.-P.; Graham, M. D.; De Pablo, J. J. *J. Chem. Phys.* **2006**, *125*, 164906.
(44) Hernández-Ortiz, J.-P.; de Pablo, J. J.; Graham, M. D. *Phys. Rev. Lett.* **2007**, *98*, 140602.
(45) Khare, R.; Graham, M. D.; de Pablo, J. J. *Phys. Rev. Lett.* **2006**, *96*, 224505.

MA070729T